Negative refraction in gyrotropic media

V. M. Agranovich,[1,2] Yu. N. Gartstein,[3] and A. A. Zakhidov[1,3]
[1]*UTD-NanoTech Institute, The University of Texas at Dallas, Richardson, Texas 75083, USA*
[2]*Institute of Spectroscopy, Russian Academy of Science, Troitsk, Moscow*
[3]*Department of Physics, The University of Texas at Dallas, Richardson, Texas 75083, USA*
(Received 23 September 2005; revised manuscript received 7 November 2005; published 18 January 2006)

The gyrotropy (chirality) as one of the manifestations of spatial dispersion responsible, e.g., for the rotation of the plane of polarization of light can also lead to negative refraction (NR) in certain frequency ranges. We discuss this effect for homogeneous isotropic chiral media in a nonresonant frequency domain close to frequency ω_L of longitudinal excitations, where dielectric permittivity vanishes: $\epsilon(\omega_L)=0$. Basic phenomena of reflection and refraction at the boundary of a chiral medium are considered and NR is demonstrated for frequencies below ω_L as following from the negative group velocity of circularly polarized electromagnetic waves of one handedness. We show that specular reflection of the polarized waves should provide a means of direct experimental detection of this frequency domain. We also discuss dissipation-related limitations for realization of NR.

DOI: 10.1103/PhysRevB.73.045114 PACS number(s): 78.20.Ek, 42.25.Gy, 33.55.Ad, 42.25.Bs

I. INTRODUCTION

Because of both fundamental and practical importance, there has been an explosion of interest in left-handed materials (LHM's) predicted by Veselago[1] which are also known now as negative refraction (NR) materials. In his paper Veselago[1] considered homogeneous isotropic media having simultaneously negative dielectric permittivity $\epsilon(\omega)$ and magnetic permeability $\mu(\omega)$. The experiments for microwave frequencies performed in different laboratories proved experimentally that negative refraction can be achieved using split-ring resonator (SRR) arrays embedded into metallic meshes. Very convincing results on negative refraction have been as well obtained for a three-dimensional (3D) version of SRR arrays. Also for microwaves and recently[2] for IR, the negative refraction has been demonstrated in a quite different class of materials, photonic crystals. Discussion of the results obtained for the mentioned artificial materials can be found, for instance, in recent review papers[3–6] and a contributed volume.[7] It is important, however, to stress that the NR of electromagnetic waves may also exist in nature and even with magnetic permeability $\mu(\omega)=1$. As has been well understood long ago (see, for example, Refs. 8–10), the NR should take place for electromagnetic waves with "negative group velocity" $\mathbf{v}_g$ — that is, when $\mathbf{v}_g(\mathbf{k})=\partial\omega(\mathbf{k})/\partial\mathbf{k}$ is directed opposite to the direction of wave vector $\mathbf{k}$. All unusual properties of NR materials are a very natural consequence of such a relationship. The Poynting vector $\mathbf{S}$ for a wave packet is a product of the electromagnetic energy density u and the wave group velocity,[10] $\mathbf{S}=u\mathbf{v}_g$, and thus the group velocity rather than the wave vector determines the direction of energy flow (assuming a negligible dissipation). In isotropic media to which we will restrict our consideration here, the Poynting vector can be directed along $\mathbf{k}$ or $-\mathbf{k}$. The former is the case of a familiar "positive" refraction. The latter case of negative refraction is possible if the dielectric permittivity of the medium exhibits strong enough spatial dispersion.[11] Spatial dispersion signifying a nonlocal dielectric response is reflected in a dependence of the generalized dielectric tensor $\epsilon_{ij}(\omega,\mathbf{k})$ on wave vector $\mathbf{k}$.[12] Discussion of effects of spatial dispersion requires therefore a knowledge of the dependence of $\epsilon_{ij}(\omega,\mathbf{k})$ not only on frequency ω but also on wave vector $\mathbf{k}$. The consideration is simplified whenever the spatial dispersion is determined by a small parameter $ka\sim a/\lambda\ll 1$, where a is the length on the order of a lattice constant (or of a mean free path of charge carriers in conducting media) and λ the wavelength of light in the medium. The smallness of ka allows us to use only the first terms (linear and/or quadratic) in the expansion of the tensor $\epsilon_{ij}(\omega,\mathbf{k})$ [or of its inverse $\epsilon_{ij}^{-1}(\omega,\mathbf{k})$] in power series of the components of the wave vector $\mathbf{k}$.[10,12]

The importance of the role of the spatial dispersion depends on the frequency ω. Consider for clarity an isotropic medium. In the absence of spatial dispersion, the dielectric tensor for transverse waves would then reduce to $\epsilon(\omega)\delta_{ij}$ where $\epsilon(\omega)$ signifies a "usual" frequency dispersion of the permittivity. Evidently one can expect that the spatial dispersion corrections to the tensor $\epsilon_{ij}(\omega,\mathbf{k})$ may become especially important in the vicinity of the frequency with vanishing $\epsilon(\omega)=0$. Likewise, spatial dispersion corrections to the tensor $\epsilon_{ij}^{-1}(\omega,\mathbf{k})$ can be important near resonances of $\epsilon(\omega)$. This latter case of small $1/\epsilon(\omega)$ was specifically discussed in Ref. 10, including the appearance of waves with negative group velocity and negative refraction in chiral media.[35] In this paper we will be concerned with *transverse* electromagnetic waves within a range of frequencies around ω_L such that $\epsilon(\omega_L)=0$. ω_L is thus the frequency of the longitudinal electromagnetic wave; we will be calling ω_L the longitudinal frequency for short. Particularly we will be discussing transverse waves with negative group velocity that may arise in natural gyrotropic (chiral) media.

A "chiral route" to negative refraction in the vicinity of the longitudinal frequency has been specifically emphasized by Pendry[3] in the context of artificial metamaterials in the microwave diapason. Related is the recent theoretical work on negative refraction in chiral materials with certain mate-

rial parameters[13,14] including demonstrations of focusing for circularly polarized waves.[15,16] The phenomena of natural optical activity and circular dichroism, associated with chirality, have been long known for natural materials at optical frequencies. With optical diapason applications in mind, we find it appropriate to follow discussions of the optics of chiral media[10,12,17,18] within the framework conveniently provided by the generalized dielectric tensor $\epsilon_{ij}(\omega,\mathbf{k})$. This approach has at its basis an important physical consideration that, at optical frequencies, the notion of magnetic permeability loses its conventional physical meaning[12] (see Sec. II A). The framework is applicable for both microwave and optical frequency domains as well as for various types of spatial dispersion, allowing us to discuss negative refraction on the same footing in both chiral and achiral media.[11,19,20] It is the spatial dispersion approach that we use in this paper to analyze the response of the chiral medium in the nonresonant frequency domain in the vicinity of ω_L. Different from the work mentioned above[3,13–16] is also our emphasis on the discussion of the frequency dependence of responses both below ω_L (where negative group velocity waves occur) and above ω_L. The consideration will mostly be restricted to the description of the picture expected for negligible dissipation. We will, however, also provide a brief discussion of dissipation effects and the important constraints they impose on material parameters.

II. ELECTROMAGNETIC WAVES IN GYROTROPIC ISOTROPIC MEDIA

A. Spatial dispersion

In gyrotropic media the spatial dispersion manifests itself already in terms of a first-order smallness with respect to the wave vector $\mathbf{k}$ (first-order terms would disappear in the absence of chirality owing to symmetry considerations). Keeping only terms linear in $\mathbf{k}$ components, the expansion of the permittivity tensor takes the form[12]

$$\epsilon_{ij}(\omega,\mathbf{k}) = \epsilon_{ij}(\omega) + i\gamma_{ijl}(\omega)k_l. \tag{1}$$

Correspondingly, the electric displacement $\mathbf{D}(\omega,\mathbf{k})$ is related to the electric field $\mathbf{E}$ through

$$D_i = \epsilon_{ij}(\omega)E_j + i\gamma_{ijl}(\omega)E_jk_l. \tag{2}$$

With spatial dispersion of the dielectric tensor taken into account, there is no need to consider separately (that is, in addition to the induction $\mathbf{B}$) the magnetic field $\mathbf{H}$: $\mathbf{H}=\mathbf{B}$.[12] As applied to nonferromagnetic bodies, this approach does not affect the generality of the theory and its especial appropriateness for optical frequencies has been lucidly demonstrated in a textbook description.[12] In that range of frequencies, quoting from Ref. 12, "…the effects due to the difference of μ from unity are in general indistinguishable from those of the spatial dispersion of the permittivity" and "Instead, all terms which result from averaging the microscopic currents are included in the definition of $\mathbf{D}$."

Interestingly, a debate over "correctness" and "appropriateness" of different approaches has been quite long particularly in connection with the gyrotropic media (more precisely, with the optics at the boundaries of such media) and we refer the reader to recent accounts[21–23] listing multiple original papers. It is well recognized that, in the region of applicability of different approaches, equivalent results are obtained when appropriate boundary conditions are used. The latter in fact have been extensively discussed in a monograph[10] for boundaries of different media with spatial dispersion (see also below). We refrain from a discussion of the formal criteria of convenience of using this or that approach but would like to stress the relationship of the generalized permittivity tensor $\epsilon_{ij}(\omega,\mathbf{k})$ to the dispersion of the elementary excitations (excitons) in the medium, allowing, in principle, its direct microscopic calculation.[10] As applied to the issues of negative group velocity and negative refraction, the usefulness of the approach we use in this paper has already been demonstrated.[10,11,19,20]

In the isotropic medium the structure of tensors ϵ_{ij} and γ_{ijl} reduces to that of elementary tensors,[10,12] $\epsilon_{ij}(\omega) = \epsilon(\omega)\delta_{ij}$, $\gamma_{ijl}=\gamma(\omega)e_{ijl}$, and Eq. (2) becomes

$$\mathbf{D} = \epsilon(\omega)\mathbf{E} + i\gamma(\omega)\mathbf{E}\times\mathbf{k}; \tag{3}$$

see also parallel textbook discussions in Refs. 17 and 18. Maxwell equations for the plane waves, on the other hand, result in

$$\mathbf{D} = \frac{k^2c^2}{\omega^2}[\mathbf{E} - \mathbf{k}(\mathbf{kE})/k^2]. \tag{4}$$

Equations (3) and (4) together determine then the dispersion relations for two transverse ($\mathbf{kE}=0$) circularly polarized waves as obeying

$$\epsilon(\omega) - (c^2k^2/\omega^2) = \pm|\gamma(\omega)|k, \tag{5}$$

where $k=\sqrt{\mathbf{k}^2}$ is the magnitude of the wave vector. The longitudinal waves ($\mathbf{D}=0, \mathbf{E}\|\mathbf{k}$) meanwhile satisfy $\epsilon(\omega)=0$ at $\omega=\omega_L$. "Plus" and "minus" branches in Eq. (5) correspond to polarizations of opposite handedness. For certainty, we will be assuming below that $\gamma>0$; then, the "plus" branch corresponds to left-hand polarized waves while the "minus" branch to right-hand waves. (The assignment of polarizations would be opposite for $\gamma<0$.) Without loss of generality we will choose waves vectors $\mathbf{k}$ to be in xz plane. Then $\mathbf{k}=k_x\hat{\mathbf{x}} + k_z\hat{\mathbf{z}}, k=\sqrt{k_x^2+k_z^2}$ and left- and right-hand polarization vectors of the electric field can be conveniently chosen as

$$\mathbf{e}_{\pm}(\mathbf{k}) = \frac{k_z}{k}\hat{\mathbf{x}} \pm i\hat{\mathbf{y}} - \frac{k_x}{k}\hat{\mathbf{z}}. \tag{6}$$

As left- and right-hand polarized waves propagate with different phase velocities, a linearly polarized light will be experiencing the rotation of its plane of polarization equal to

$$\rho = \frac{\gamma\omega^2}{2c^2} \tag{7}$$

per the unit length of ray passage (see, e.g., Ref. 12 and below), ρ being the rotatory power of the chiral medium. Thus, experimental data on the rotatory power in gyrotropic materials can be used for estimates of the magnitude of spatial dispersion effects. One however has to keep in mind that,

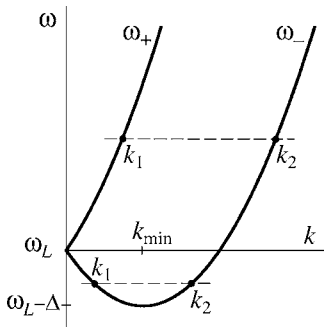

FIG. 1. Frequencies of the normal transverse waves in the chiral medium in the vicinity of ω_L as functions of the wave vector magnitude $k=\sqrt{\mathbf{k}^2}$. Two waves characterized by k_1 and k_2 are shown each for some frequencies (dashed lines) above and below ω_L. k_1 waves at $\omega<\omega_L$ are those with negative group velocities.

along with permittivity $\epsilon(\omega)$, constant $\gamma(\omega)$ can depend on the wave frequency ω.

B. Dispersion relations for transverse waves in the vicinity of longitudinal frequency ω_L

We now restrict, for clarity of expressions only, our explicit consideration of transverse waves to a range of frequencies around the longitudinal frequency, where the dielectric permittivity can be approximated as a linear function

$$\epsilon(\omega) \simeq A_L(\omega-\omega_L), \quad A_L = \left.\frac{\partial\epsilon(\omega)}{\partial\omega}\right|_{\omega=\omega_L} > 0, \tag{8}$$

which vanishes exactly at ω_L: $\epsilon(\omega_L)=0$. More precisely, it is the real part of $\epsilon(\omega)$ that vanishes at ω_L (see Sec. II C). The corresponding value of the gyrotropic parameter γ is now at that frequency: $\gamma=\gamma(\omega_L)$.

With $\epsilon(\omega)$ from Eq. (8) the dispersion relations (5) as functions of $k=\sqrt{\mathbf{k}^2}$ for the normal transverse waves in the chiral medium take a simple form of "displaced parabolas":

$$\omega_\pm(k) \simeq \omega_L + \frac{c^2}{A_L\omega_L^2}k^2 \pm \frac{\gamma}{A_L}k, \tag{9}$$

as illustrated in Fig. 1. Evidently, for each frequency ω, where waves can exist there are two types of solutions with k values denoted k_1 and k_2 such that $k_1 \leqslant k_2$. For frequencies $\omega>\omega_L$, k_1 and k_2 waves belong to different polarization branches [$\omega_+(k)$ and $\omega_-(k)$], while at $\omega<\omega_L$, they belong to the same branch $\omega_-(k)$. The latter has a minimum of $\omega_-(k_{\min})=\omega_L-\Delta$ (the bottom of the allowed frequencies for the propagating waves) achieved at $k=k_{\min}\simeq(\omega_L^2/2c^2)\gamma$. The depth of this minimum,

$$\Delta = \omega_L - \omega_-(k_{\min}) \simeq \gamma^2\omega_L^2/4A_Lc^2, \tag{10}$$

strongly depends not only on ω_L and γ but also on value A_L. It is clear from Fig. 1 that it is the part $\omega_-(k<k_{\min})$ (k_1 waves) at $\omega<\omega_L$ which exhibits negative group velocities as the frequency in that part decreases with growing wave vector k_1. All other parts of the spectrum (9) have the usual positive group velocities. At the bottom of the allowed frequency range $\omega_L-\Delta$, $k_1=k_2=k_{\min}$ and both waves have a vanishing group velocity. (As discussed later, we will find it more convenient to extend the definition of k_1 to allow it to become negative for a description of negative group velocity waves.) Needless to say that the accuracy of expression (10) for Δ assumes that the minimum is reached still within the region of validity of approximation (8).

It is useful to notice that an exact [for unspecified ω dependences of $\epsilon(\omega)$ and $\gamma(\omega)$] relationship follows from Eq. (5) for the difference between wave vector magnitudes at the same frequency $\omega>\omega_L$,

$$k_2 - k_1 = \gamma\omega^2/c^2, \tag{11}$$

and its exact counterpart for frequencies $\omega<\omega_L$ relates the sum of wave vector magnitudes at the same frequency:

$$k_2 + k_1 = \gamma\omega^2/c^2. \tag{12}$$

It should also be noted that small changes of frequency ω around ω_L may result in relatively large changes of wave vector magnitudes k_1 and k_2. While still compatible with $ka\ll 1$, the value of $k_{\min}$ can, at this level of discussion, be larger or smaller than the wave vector ω_L/c of the corresponding electromagnetic wave in vacuum. In other words, the dimensionless parameter

$$\gamma' = \gamma\omega_L/c \tag{13}$$

may, in principle, be either smaller or larger than 1. We expect that for a majority of natural media γ' is very small but could be made larger in artificial metamaterials. Of course, in the case of large γ', one would need to verify the relevance of higher-order terms in expansion (1) in wave vector components, which we do not consider here.

C. Constant A_L and dissipation

For the isotropic dielectric medium with a single (oscillator) resonance frequency ω_T, the dielectric permittivity in the vicinity of ω_L is known to be

$$\epsilon(\omega) = \epsilon_b\left(\frac{\omega^2-\omega_L^2+2i\omega\Gamma}{\omega_L^2-\omega_T^2}\right) \simeq \frac{\epsilon_b}{\omega_L-\omega_T}(\omega-\omega_L+i\Gamma), \tag{14}$$

where ϵ_b is the background dielectric constant and Γ the dissipative width. It follows from Eq. (14) that in the oscillator model constant

$$A_L = \frac{\epsilon_b}{\omega_L-\omega_T}$$

and the depth of the minimum (10) is

$$\Delta = \frac{\gamma^2\omega_L^2(\omega_L-\omega_T)}{4\epsilon_b c^2}. \tag{15}$$

For the free electrons in the Drude model,

$$\epsilon(\omega) = \epsilon_b - \frac{\omega_p^2}{\omega(\omega+i\Gamma_p)}, \tag{16}$$

where ω_p is the plasma frequency and Γ_p the frequency of electron collisions in plasma. It follows from Eq. (16) that

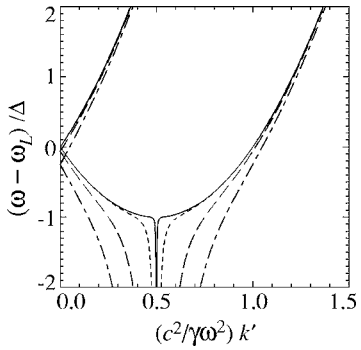

FIG. 2. Dissipation-related modification of the dispersion of the transverse waves in the chiral medium in the vicinity of ω_L; compare to Fig. 1: Here it is shown in a dimensionless form for $\omega(k')$. Different lines correspond to different magnitudes of the relative dissipation Γ/Δ: 0.01 (solid line), 0.1 (short-dashed line), 0.5 (long-dashed line), and 1.0 (dash-dotted line).

$$\omega_L \simeq \frac{\omega_p}{\sqrt{\epsilon_b}}, \quad A_L \simeq \frac{2\epsilon_b^{3/2}}{\omega_p}.$$

Thus, for the plasma model, the depth of the minimum (10) is

$$\Delta = \frac{\gamma^2 \omega_p^3}{8\epsilon_b^{5/2} c^2}. \tag{17}$$

As should be clear from the above, the result (10) for Δ and concomitant Eqs. (15) and (17) have been derived neglecting the effects of dissipation. The dispersion of the waves shown in Fig. 1 retains its physical significance only if the minimum depth Δ is large enough in comparison with the dissipative width Γ of *transverse* electromagnetic waves in the region of frequencies around ω_L. Indeed, with Γ taken into account the wave vector becomes complex and, for homogeneous plane waves, one has

$$k = k' + ik''.$$

As an example, let us take the oscillator model, Eq. (14), for which the dispersion equation (5) would now read

$$c^2(k'^2 - k''^2)/\omega^2 \pm \gamma k' = A_L(\omega - \omega_L),$$

$$2c^2 k' k''/\omega^2 \pm \gamma k'' = A_L \Gamma. \tag{18}$$

Already assuming frequencies ω to be in the vicinity of ω_L, Eqs. (18) are amenable to scaling all the frequencies in terms of Δ, Eq. (10), and all the wave vectors in terms of $k_{\min}$. Modifications of the dispersion relations $\omega(k')$ following from Eqs. (18) are shown in Fig. 2 for several values of dimensionless Γ/Δ. It is clear from Fig. 2 that, except in the immediate vicinity of the dispersion minimum itself, deviations of the dispersion relations caused by the dissipation are negligible for $\Gamma/\Delta \ll 1$. This condition, however, imposes strong material limitations. (A discussion of optical properties in the presence of strong dissipation effects is outside the scope of this paper.)

Together with a descriptive model restriction, the oscillator model result (15), for instance, would then be limited to such a region of parameters that

$$\omega_L - \omega_T \gg \Delta \gg \Gamma. \tag{19}$$

The first inequality here follows from the applicability of approximation (8). This approximation is, of course, not principal and has been used in this section only to clearly show the resulting qualitative behavior of the wave dispersion.

III. REFLECTION AND REFRACTION OF ELECTROMAGNETIC WAVES

In this section we will be concerned with reflection and refraction of waves occurring at the boundary between a normal medium (vacuum) and the chiral medium described above. A proper consideration of reflection and refraction requires using correct boundary conditions for the electric and magnetic fields. This subject has actually been quite contentious[21–23] despite the fact that its foundation was established a long time ago.[10] Below we give a brief exposition of the issue of boundary conditions in the formalism we use as applicable to the problem at hand.

A. Boundary conditions

First of all, it should be noted that in the frequency range around ω_L for each frequency ω there exist only two branches of normal modes with different values of wave vector magnitudes. As will be clear from the examples considered in the following subsections, two waves in the chiral medium involved in the basic refraction process have opposite-handedness polarization. This particularly means that we do not deal here with a situation where the spatial dispersion is responsible for the appearance of so-called additional electromagnetic waves of the same polarization. It is known[10] that in such cases the usual Maxwell boundary conditions are not sufficient to find amplitudes of all the waves and an additional boundary condition (ABC) has to be used. The form of the ABC strongly depends on the nature of elementary excitations in the medium and is, for instance, different for Frenkel and Wannier-Mott excitons. For nongyrotropic crystals, the effect of new waves near resonances of the dielectric tensor was originally predicted by Pekar[24] in 1957 who also was the first to propose a form of an additional boundary condition (Pekar's ABC). For gyrotropic materials the same effect was demonstrated by Ginzburg.[25] Propagation of optical waves in gyrotropic crystals under such conditions has been discussed in Ref. 10, including waves with negative group velocities.

Even though uncomplicated in our case by additional waves, boundary conditions for the medium with the spatial dispersion in the formalism we use generally differ from the familiar Maxwell boundary conditions of continuity for tangential components of the electric **E** and magnetic **H** fields (see also Refs. 21–23). For the boundary between regular and chiral media, one can show that while the tangential components of the electric field remain continuous,

$$\mathbf{E}_t' = \mathbf{E}_t, \tag{20}$$

the tangential components of the magnetic field of the monochromatic wave exhibit a discontinuity:

$$\mathbf{B}_t' = \mathbf{B}_t + \frac{i\gamma\omega}{2c}\mathbf{E}_t. \tag{21}$$

In Eqs. (20) and (21) we used a prime to denote the fields on the side of the chiral medium. Discontinuity (21) is caused by the surface currents on the interface. A transparent way to see the appearance of discontinuity (21) is to realize that in a chiral medium with *spatially variable* chiral constant γ, all spatial derivatives should be considered on the same footing and the relationship between $\mathbf{D}$ and $\mathbf{E}$ must also contain spatial derivatives of γ. The principle of symmetry of kinetic coefficients then requires[10,26] a modification of Eq. (3) to

$$\mathbf{D} = \epsilon(\omega)\mathbf{E} - \gamma\boldsymbol{\nabla} \times \mathbf{E} - \frac{1}{2}(\boldsymbol{\nabla}\gamma) \times \mathbf{E}. \tag{22}$$

The boundary between chiral and regular media is a particular case of spatial variation of γ. The last term in Eq. (22) immediately gives rise to the discontinuity in boundary condition (21) when Maxwell's equation $c\boldsymbol{\nabla} \times \mathbf{B} = \partial\mathbf{D}/\partial t$ with $\mathbf{D}$ from Eq. (22) is integrated over an infinitely thin transition layer between a regular medium with $\gamma = 0$ and a chiral medium with finite γ. It is also easily seen that condition (21) guarantees the continuity of the energy flux across the interface. On the side of the regular medium the energy flux has a familiar form ($\mathbf{B} = \mathbf{H}$)

$$\mathbf{S} = \frac{c}{8\pi}\mathrm{Re}(\mathbf{E}^* \times \mathbf{B}), \tag{23}$$

while on the side of the medium with the spatial dispersion is expressed as[10,12]

$$\mathbf{S}' = \frac{c}{8\pi}\mathrm{Re}(\mathbf{E}'^* \times \mathbf{B}') - \frac{\omega}{16\pi}\frac{\partial\epsilon_{ik}}{\partial\mathbf{k}}E_i'^* E_k'. \tag{24}$$

The latter term in Eq. (24) for our chiral medium becomes just

$$-\frac{i\gamma\omega}{16\pi}\mathbf{E}'^* \times \mathbf{E}'. \tag{25}$$

As the tangential component of the electric field is continuous at the interface, Eq. (20), discontinuity (21) is exactly what ensures the continuity of the normal component of the flux, $\mathbf{S}_n = \mathbf{S}_n'$, by canceling the effect of the spatial dispersion correction (25).

B. Boundary between semi-infinite media

We will proceed here with the reflection and refraction of waves at the interface separating two semi-infinite spaces: regular (say, vacuum, for simplicity) at $z < 0$ and our chiral medium at $z > 0$, as schematically shown in Fig. 3. This is a "standard" problem, and its treatment for the usual range of frequencies away from ω_L within the symmetric formalism can be found, e.g., in Refs. 27 and 28. Let an electromagnetic

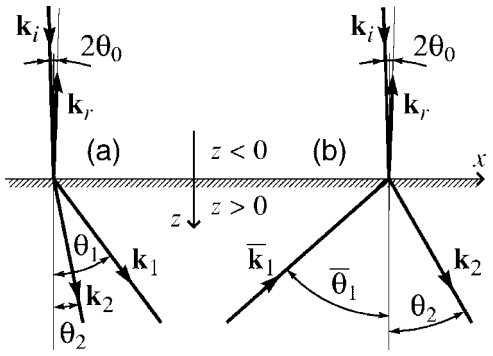

FIG. 3. Reflection and refraction of a plane electromagnetic wave at the interface between a regular medium (vacuum), $z < 0$, and the chiral medium, $z > 0$, for the case of the chiral medium being optically less dense for both refracted waves. Incident angle θ_0 here is small enough for both waves to be excited in the medium. The left part (a) corresponds to frequencies $\omega > \omega_L$ where both k_1 and k_2 waves have positive group velocities. The right part (b) corresponds to frequencies $\omega < \omega_L$ with one of the refracted waves ($\bar{\mathbf{k}}_1$) having a negative group velocity. Only the directions of wave vectors are shown in this figure. The direction of the energy flow $\mathbf{S}$ for the $\bar{\mathbf{k}}_1$ wave is opposite to the direction of the wave vector.

wave of frequency ω (and wave vector magnitude $k_0 = \omega/c$) be incident from the vacuum onto the interface at angle θ_0. Let us choose the plane of incidence to be the xz plane so that all wave vectors involved have only x and z components. There are in fact four wave vectors involved: those of the incident and reflected waves as well as two vectors characterizing the waves excited in the chiral medium. As discussed above (see Fig. 1), for a given ω, the chiral medium supports waves with two different magnitudes of the wave vector, k_1 and k_2.

We consider the interface, $z = 0$ plane, to be uniform, which immediately leads to the conservation of x components of all wave vectors, determined therefore by that of the incident light:

$$k_{ix} = k_0 \sin\theta_0 = k_1 \sin\theta_1 = k_2 \sin\theta_2, \tag{26}$$

where θ_1 and θ_2 are the refraction angles for k_1 and k_2 waves in the medium. The reflection angle is of course just equal to θ_0. Fixing the x components this way determines in turn z components of the refracted wave vectors, as illustrated in Fig. 4. So, in a vectorial notation, the incident light wave vector is

$$\mathbf{k}_i = k_0(\sin\theta_0\hat{\mathbf{x}} + \cos\theta_0\hat{\mathbf{z}}) \tag{27}$$

and that of the reflected light

$$\mathbf{k}_r = k_0(\sin\theta_0\hat{\mathbf{x}} - \cos\theta_0\hat{\mathbf{z}}), \tag{28}$$

while two refracted wave vectors are normally

$$\mathbf{k}_1 = k_1(\sin\theta_1\hat{\mathbf{x}} + \cos\theta_1\hat{\mathbf{z}}) \tag{29}$$

and

$$\mathbf{k}_2 = k_2(\sin\theta_2\hat{\mathbf{x}} + \cos\theta_2\hat{\mathbf{z}}). \tag{30}$$

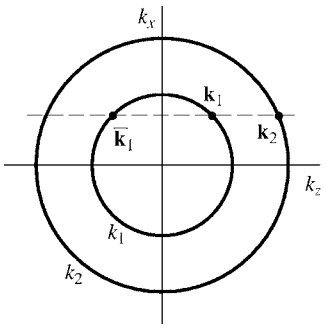

FIG. 4. Graphical determination of the z components of the refracted wave vectors given a fixed frequency and a fixed x component (dashed line) of the wave vector of the incident wave. The frequency establishes the magnitudes k_1 and k_2 of refracted wave vectors. The dashed line here allows real values of z components for both waves. Moving the line upward (that is, increasing the incident angle for a large enough incident k_0) would first prevent the k_1 wave and then both k_1 and k_2 waves from propagating in the medium.

A standard appearance of $\mathbf{k}_1$ and $\mathbf{k}_2$ in the form (29) and (30) does not require any comment at $\omega > \omega_L$ [part (a) of Fig. 3], where both waves have positive group velocities. At frequencies $\omega < \omega_L$, however, the k_1 wave has a negative group velocity and the energy flux $\mathbf{S}$ is directed against the wave vector. The principle of causality demands that the energy flux of the refracted waves can be only in the positive z direction, that of the incident wave energy flux. Therefore the z component of the $\mathbf{k}_1$ vector, k_{1z}, has to be negative at frequencies $\omega < \omega_L$. We emphasize this by denoting the refracted wave vector of the k_1 wave in that frequency range by $\bar{\mathbf{k}}_1$ in Figs. 3(b) and 4. From those figures,

$$\bar{\mathbf{k}}_1 = k_1(\sin\bar{\theta}_1\hat{\mathbf{x}} - \cos\bar{\theta}_1\hat{\mathbf{z}}), \tag{31}$$

where the angle $\bar{\theta}_1$ is considered positive but on the same side of normal as the incident ray. Obviously, $\bar{\mathbf{k}}_1$ in Eq. (31) can be rewritten in the form (29) if the definitions of k_1 and θ_1 are extended for the k_1 wave to acquire negative values at frequencies $\omega < \omega_L$ such that $-|k_1| \to k_1$ and $\bar{\theta}_1 \to -\theta_1$—that is,

$$\bar{\mathbf{k}}_1 = k_1(\sin\theta_1\hat{\mathbf{x}} + \cos\theta_1\hat{\mathbf{z}}), \tag{31a}$$

where k_1 and θ_1 are now both negative in accordance with our generalized definition. This extension agrees with Eq. (26) as well as with the relationship between Eqs. (11) and (12). In fact, as will become clear, for all our purposes we can use a unified description for frequencies both above and below ω_L with the understanding that k_1 becomes negative ("negative index of refraction" for the negative group velocity waves) for $\omega < \omega_L$. With this extended definition, the range of allowed k_1 values becomes $k_1 \geqslant -k_{\min}$, while k_2 values are still $k_2 \geqslant k_{\min}$. At the bottom of the allowed frequency range $\omega = \omega_L - \Delta$, the extended $k_1 + k_2 = 0$.

Equations (26)–(31) and (31a) are written down in the traditional form as if all the angles and wave vector components were real. Our consideration will also include cases similar to the total reflection where some wave vector z components (and, correspondingly, refraction angles) become purely imaginary; see Fig. 4. When imaginary, z components are to be taken in the upper complex half-plane to ensure a decay of waves in the chiral medium at $z > 0$.

In the immediate vicinity of medium's longitudinal frequency ω_L, k_1 waves always have small wave vectors $|k_1| \ll k_0$ and respectively small relative refraction indices. Therefore k_1 waves would not be excited in the medium already at very small incident angles. The occurrence of total-reflection-like situations for k_1 and k_2 waves at frequencies $\omega < \omega_L$ depends on the value of dimensionless parameter γ', Eq. (13)—that is, on the magnitude of $k_{\min}$ relative to incident k_0. Roughly speaking, for $\gamma' \ll 1$, both k_1 and k_2 waves can easily be prevented from propagating in the medium already at small incident angles. For $k_{\min} > k_0$, however, k_2 waves would always be excited in the medium and so would be k_1 waves for frequencies sufficiently far from ω_L.

It is convenient to work with circularly polarized waves: the incident wave electric field vector polarized as either $\mathbf{e}_+(\mathbf{k}_i)$ or $\mathbf{e}_-(\mathbf{k}_i)$ while looking for the reflected wave electric field at the interface as

$$a\mathbf{e}_+(\mathbf{k}_r) + b\mathbf{e}_-(\mathbf{k}_r) \tag{32}$$

and for that of refracted waves as

$$A\mathbf{e}_+(\mathbf{k}_1) + B\mathbf{e}_-(\mathbf{k}_2). \tag{33}$$

Equation (33) is originally valid for frequencies $\omega > \omega_L$; see assignments in Fig. 1. Coefficients a,b and A,B appearing in Eqs. (32) and (33) are to be determined from the boundary conditions (20) and (21) on the tangential (that is, x and y) components of the electric and magnetic fields. To calculate the latter from Maxwell's equation $(\omega/c)\mathbf{B} = \mathbf{k} \times \mathbf{E}$, it is handy to use the relationship

$$\mathbf{k} \times \mathbf{e}_\pm(\mathbf{k}) = \mp ik\mathbf{e}_\pm(\mathbf{k}), \quad k = \sqrt{\mathbf{k}^2}. \tag{34}$$

For $\omega < \omega_L$ it is the ω_- branch of the spectrum that is involved for both refracted waves and one, instead of Eq. (33), can write down as

$$-A\mathbf{e}_-(\bar{\mathbf{k}}_1) + B\mathbf{e}_-(\mathbf{k}_2). \tag{33a}$$

However, the first term in Eq. (33a) coming from the negative group velocity wave yields for the tangential part $-A(-\cos\theta_1\hat{\mathbf{x}} - i\hat{\mathbf{y}})$, which would be identical to the tangential part of the first term in Eq. (33), thereby providing a similar formal description above and below ω_L. It is reassuring to realize that the conclusion of k_{1z} having to be negative at $\omega < \omega_L$ following from considerations of the energy flux direction is consistent with the polarization considerations as only then $\mathbf{e}_-(\bar{\mathbf{k}}_1)$ along with $\mathbf{e}_-(\mathbf{k}_2)$ would constitute a basis sufficient to satisfy boundary conditions for arbitrary incident polarizations. From Eq. (34) it is also clear that the formal difference between boundary condition equations for $\omega > \omega_L$ and $\omega < \omega_L$ regions would be taken care of if k_1 is considered negative for the latter.

It is convenient to introduce relative refraction indices with respect to the wave vector magnitude k_0 of the incident wave,

$$n_1 = k_1/k_0, \quad n_2 = k_2/k_0 \tag{35}$$

and, further on, their average value n through

$$n_2 = n + \delta, \quad n_1 = n - \delta. \tag{36}$$

In using index n_1 we will be assuming our extension of definition of k_1 so that n_1 is negative at frequencies $\omega < \omega_L$. Note that it follows from Eqs. (11) and (12) for the extended definition that $2\delta = \gamma(\omega/c)^2/k_0$, so that in the vicinity of $\omega = \omega_L$, the difference $n_2 - n_1 \simeq \gamma k_0$ is approximately constant.

Before discussing specular incidence results, it is instructive to show in more detail the role of the discontinuity of $\mathbf{B}_t$, eq. (21), for the simpler case of normal incidence. For normal incidence, circularly polarized waves do not "mix": so for the incident $\mathbf{e}_-(\mathbf{k}_i)$ wave one would have in the reflected wave $b=0$ and $A=0$ in the refracted wave vectors $\mathbf{E}$ for all the involved waves are proportional to the $\hat{\mathbf{x}} - i\hat{\mathbf{y}}$ vector. Boundary conditions (20) and (21) result in the following equations for amplitudes:

$$B = 1 - a,$$

$$k_2 B - \frac{1}{2}(k_2 - k_1)B = k_0(1 + a). \tag{37}$$

It is the term proportional to $(k_2 - k_1)$ in eq. (37) that resulted from the discontinuity [here it was transformed using the exact relationship (11)]. In its absence, the reflection amplitude a would incorrectly be a function of n_2; with this term in place, a becomes a function of the *averaged* refraction index only:

$$B = 1 - a,$$

$$nB = 1 + a, \tag{37a}$$

so that

$$a = \frac{n-1}{n+1}. \tag{38}$$

For the normally incident $\mathbf{e}_+(\mathbf{k}_i)$ wave, the same ratio (38) of course results but for the amplitude b (for this polarization $a=B=0$). These relationships hold for both frequencies above and below ω_L when n is understood in the discussed extended definition. It is particularly clear that no rotation of the plane of polarization occurs for a linearly polarized light upon reflection at normal incidence and that the differential reflectance of circularly polarized waves (the relative difference of reflectances for left- and right-hand polarized waves) is zero.[27]

For the general specular incidence circular polarizations mix resulting in coupling between all the amplitudes, instead of system (37a) for the incident $\mathbf{e}_-(\mathbf{k}_i)$ wave one gets

$$A \cos\theta_1 + B \cos\theta_2 = \cos\theta_0(1 - a - b),$$

$$A - B = -1 + a - b,$$

$$n(-A \cos\theta_1 + B \cos\theta_2) = \cos\theta_0(1 + a - b),$$

$$n(A + B) = 1 + a + b. \tag{39}$$

Set (39) is easily solved to find for the reflection amplitudes

$$b = \frac{4n}{(1-n)^2 f_1 - (1+n)^2/f_2} \tag{40}$$

and

$$a = \frac{n-1}{n+1}(1 + f_1 b), \tag{41}$$

where

$$f_i = \frac{\cos\theta_i - \cos\theta_0}{\cos\theta_i + \cos\theta_0}.$$

The refracted amplitudes are determined by a and b in Eqs. (40) and (41):

$$2nA = (1-n)(1+b) + (1+n)a,$$

$$2nB = (1+n)(1+b) + (1-n)a. \tag{42}$$

For the incident $\mathbf{e}_+(\mathbf{k}_i)$ polarization, one easily finds an "inverse" result for amplitudes requiring just mutual exchanges of parameters in eqs. (40)–(42):

$$a \rightleftharpoons b, \quad \theta_1 \rightleftharpoons \theta_2, \quad A \rightleftharpoons B. \tag{43}$$

The results (40)–(43) hold for frequencies both above and below ω_L as discussed and are sufficient to calculate the characteristics of reflected and refracted waves for arbitrary incident polarizations. We would like to reiterate that no reference is made in these equations to particular approximations for ω dependences of $\epsilon(\omega)$ and $\gamma(\omega)$. In general, the reflected light has an elliptical polarization.[28] We will restrict our attention in this paper to the overall reflectance of the incident linearly polarized light for the polarizations perpendicular and parallel to the plane of incidence as shown in Figs. 5 and 6.

Consistently with our aims these figures show variations of the specular reflectance at a fixed incidence angle θ_0 as the frequency ω of the incident light is scanned from below ω_L to above ω_L. Instead of using directly ω, x axes of these figures are representative of ω through the average relative refraction index $n=(n_1+n_2)/2$. As ω is scanned up from the bottom of the allowed frequency range (see Fig. 1), n will be scanned up from zero ($n_1=-n_2$). At $\omega=\omega_L, n_1=0$. Since $n_2 - n_1 \simeq \gamma k_0$ in the vicinity of ω_L, this difference $n_2 - n_1$ serves as a measure of the chirality. Of course, this representation of the frequency dependence with a fixed angle of incidence assumes that the range of variation of frequency is much smaller than the frequency itself (the range of variation of k_0 is correspondingly much smaller than k_0 itself). Particularly this implies that $\Delta \ll \omega_L$.

Figure 5 deals with smaller magnitudes of chirality, $\gamma' \ll 1$, and a very small incident angle. The benchmark behavior with zero chirality is displayed in panel (a); it is evident that for $\sin\theta_0 > n$, a total reflection occurs. A typical Brewster angle behavior takes place with the parallel polarization reflectance vanishing very close to the total reflection ω. The picture changes substantially for nonzero chirality. A general

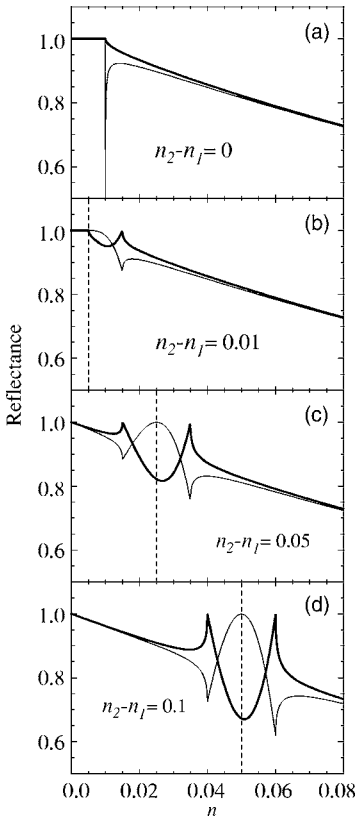

FIG. 5. Reflectance of the light polarized linearly perpendicular (thick lines) and parallel (thin lines) to the plane of incidence as a function of the average relative refraction index $n=(n_2+n_1)/2$. For all panels (a)–(d), the incident angle is fixed at $\sin\theta_0=0.01$. Panels differ by the magnitude of the chirality ($\gamma' \ll 1$) represented here as the difference n_2-n_1 of the refraction indices of waves of opposite handedness in the chiral medium. The x axis is representative of the frequency of the incident wave with $n=0$ corresponding to the bottom of the allowed frequencies for propagating waves at normal incidence. The position of ω_L corresponding to $n_1=0$ is shown by vertical dashed lines, on the left of these lines $\omega<\omega_L$ and $n_1<0$. Panel (a) shows the picture for the achiral medium, $\gamma=0$, in the vicinity of ω_L corresponding in this case to $n=0$. The incident angle is the Brewster angle in the achiral medium for n very close to 0.01 where the parallel reflectance vanishes, while rising to total reflection 1.0 at exactly $n=\sin\theta_0=0.01$.

point should be quite clear (see also Ref. 28): for a given frequency ω, in the chiral medium there would be two "total reflection angles": one corresponding to the relative refraction index n_1 (smaller critical $\sin\theta_0=|n_1|$) and the other to the relative refraction index n_2 (larger critical $\sin\theta_0=n_2$). Only beyond the latter does a "true" (complete) total reflection occur, while between those two, the k_2 wave would still be propagating in the medium. This behavior is echoed in the frequency dependence at a fixed incident angle. For clarity, let us comment for the example of particular numerical values of parameters in Fig. 5, where $\sin\theta_0=0.01$. Evidently, only for $|n_1|>0.01$ would both k_1 and k_2 waves be refracted into the medium. In the case of panel (b) ($n_2-n_1=0.01$) this is possible only for frequencies $\omega>\omega_L$. In this case, refraction of the k_2 wave happens to start exactly at ω_L where $n_1=0$ and $n_2=0.01$. At a higher frequency the k_1 wave "picks up," where $n_1=0.01$ and correspondingly $n=0.015$. This point is clearly seen through sharp signatures of the reflectance frequency dependence pattern.

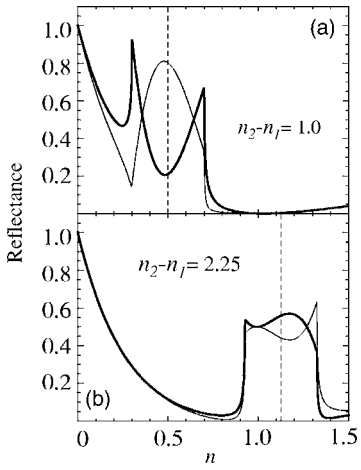

FIG. 6. As in Fig. 5 but for much stronger chirality $\gamma' \gtrsim 1$. The fixed incident angle for both panels is also larger here: $\sin\theta_0=0.2$.

Especially illuminating patterns are those displayed in panels (c) and (d) of Fig. 5 as they arise due to the fact that condition $\sin\theta_0=|n_1|$ for the critical angle of total reflection for k_1 waves can be met both below ω_L, $n_1=-\sin\theta_0$, and above ω_L, $n_1=+\sin\theta_0$. The incident frequencies between the corresponding two limiting frequencies constitute a "forbidden window" around ω_L for k_1 waves at the given incident angle when k_1 waves experience a total reflection and the $k_{1z}=+i|k_{1z}|$ component is purely imaginary. The disappearance and reemergence of k_1-wave propagation in the medium as the frequency rises are accompanied by sharp signatures of the reflectance curves. The point $\omega=\omega_L$ is also (approximately) featured through smooth extrema of the reflectance as is obvious from Fig. 5; at this point, the decay of the k_1 wave inside the medium is the fastest with $k_{1z}=ik_{ix}$. In Fig. 5, $\sin\theta_0=0.01$; hence, critical frequencies correspond to $n_1=-0.01$ below ω_L and $n_1=0.01$ above ω_L. For panel (c), for instance, one would then have critical $n=0.015$ and $n=0.035$, respectively. Needless to say that this pattern of disappearance and reemergence is possible only for such incident angles that the conserved x component of the incident wave vector $k_{ix}<k_{\min}$ (see Fig. 1)—that is, when $\sin\theta_0<(n_2-n_1)/2$ in terms of Fig. 5, which is the case for its panels (c) and (d).

For completeness, in Fig. 6 we also present the pictures of polarized reflectance for much larger values of the chirality parameter, $\gamma' \gtrsim 1$. The features discussed above around ω_L are also clearly present here. The separation between the features is larger in Fig. 6 than in Fig. 5 because of the larger incident angle, $\sin\theta_0=0.2$. The magnitudes of relative refraction indices here are large enough for this figure to display the region of average n around 1. We recall that for normal incidence, it is $n=1$ that corresponds to zero reflectance, Eq. (38). Above $n=1$, overall reflectance starts rising again, which is also reflected in Fig. 6.

Figures 5 and 6 demonstrate that already direct overall specular reflectance spectra for the polarized incident light can exhibit signatures clearly delineating an interesting range

of frequencies ω around the longitudinal frequency ω_L in the chiral medium. That includes region $\omega<\omega_L$ featuring waves with negative group velocities.

C. Transmission through a slab: Normal incidence

We will now briefly discuss normal incidence reflection and transmission of light for a chiral slab of finite thickness L; let it be the region of $0\leqslant z\leqslant L$ (see also Ref. 28). As we discussed above, at normal incidence there is no mixing of opposite-handedness circular polarizations and one can consider left- and right-hand polarizations separately. So for the incident wave with the electric field vector polarized as $\mathbf{e}_-(\mathbf{k}_i)$ all the waves involved would have vector $\mathbf{E}$ proportional to $\hat{\mathbf{x}}-i\hat{\mathbf{y}}$. The amplitude parts can be respectively written as

$$e^{ik_0z}-ae^{-ik_0z} \tag{44}$$

for $z\leqslant 0$ (incident and reflected waves),

$$Be^{ik_2z}-Ce^{-ik_1z} \tag{45}$$

for $0\leqslant z\leqslant L$ (waves in the chiral slab), and, finally,

$$De^{ik_0(z-L)} \tag{46}$$

for $z\geqslant L$ (transmitted wave). While requiring no comment for frequencies $\omega>\omega_L$, set (44)–(46) is applicable for frequencies $\omega<\omega_L$ as well if k_1 appearing in Eq. (45) is understood as negative for that frequency range. We already discussed this extension of the definition of k_1 and, once again, reassuringly, this conclusion on the sign of k_{1z} in Eq. (45) for waves with negative group velocities at $\omega<\omega_L$ consistently follows from considerations of both the energy flux direction [C term in Eq. (45) represents the wave reflected from $z=L$ boundary; hence, the energy should flow in the negative z direction] and polarization requirements. The amplitudes a, B, C, and D appearing in Eqs. (44)–(46) are to be determined from the boundary conditions (20) and (21) applied at $z=0$ and $z=L$ boundaries resulting in the following set of equations:

$$\begin{aligned} B-C&=1-a,\\ n(B+C)&=1+a,\\ Be^{i\kappa n_2}-Ce^{-i\kappa n_1}&=D,\\ n(Be^{i\kappa n_2}+Ce^{-i\kappa n_1})&=D, \end{aligned} \tag{47}$$

where we introduced $\kappa=k_0L$ in addition to definitions (35) and (36). It should be clear that for the incident wave polarized as $\mathbf{e}_+$, the difference from the description in Eqs. (44)–(46) is essentially only in the exchange $k_1\rightleftharpoons k_2$—that is, $n_1\rightleftharpoons n_2$ for set (47) [or, from definition (36), $\delta\rightarrow-\delta$]. We can then write down resulting reflection and transmission amplitudes simultaneously for $\mathbf{e}_\pm(\mathbf{k}_i)$ incident polarizations as

$$\begin{pmatrix} a\\ D\end{pmatrix}_{\pm n}=\frac{1}{2n\cos(\kappa n)-i(n^2+1)\sin(\kappa n)} \times\begin{pmatrix} i(n^2-1)\sin(\kappa n)\\ 2ne^{\mp i\kappa\delta}\end{pmatrix}. \tag{48}$$

It is evident from Eq. (48) that a and D amplitudes satisfy the conservation of the energy flux: $|a|^2+|D|^2=1$, another testament to the correctness of boundary condition (21). The resulting transmission coefficient

$$|D|^2=\frac{4n^2}{4n^2\cos^2(\kappa n)+(n^2+1)^2\sin^2(\kappa n)} \tag{49}$$

is exactly of the same form it would be for any regular medium slab of the relative refraction index n. A known feature of Eq. (49) is the existence of interference maxima at $\kappa n=\pi l$ ($l=1, 2, 3, \ldots$), when there is no reflection and all light is transmitted through the slab.

For the linearly polarized incident light, the corresponding sums of left- and right-hand circular polarization results are to be used. As Eq. (48) shows, the reflected light retains the plane of polarization of the incident light (a is independent of the polarization), while in the transmitted light, the plane of polarization rotates proportionally to the distance travelled through the slab. The angle of rotation is given by $\kappa\delta$ as follows from $D_\pm$ in Eq. (48). According to Eqs. (11), (35), and (36), this rotation angle per unit length is exactly equal to the earlier quoted rotatory power ρ Eq. (7).

It is essential to reiterate that the discussed results apply both to frequencies above and below ω_L provided that the extended definition of n_1 being negative below ω_L is used. Noteworthy is that *no* special signatures appear at the normal incidence either in reflection or transmission (48) and (49) upon "crossing" frequency ω_L [see also the previous equation (38)].

When the incident frequency ω approaches the bottom $\omega_L-\Delta$ of the allowed frequency range from above corresponding to $n\rightarrow 0$ and vanishing group velocities for waves in the medium, the transmittance (49) becomes

$$|D|^2=\frac{1}{1+(k_0L/2)^2}.$$

This result shows that, upon increasing the slab thickness L, transmittance in this limiting regime would be falling off as an algebraic function of L. Immediately above this frequency, transmittance oscillates as a function of L for all L. Immediately below this frequency, wave vectors acquire an imaginary part and transmittance becomes an exponentially decaying function of thickness L. (This situation is also no different from the one that would occur upon approach to ω_L in the regular medium with $\gamma=0$.) Of course, the above discussion has been limited to a model behavior with negligible dissipation. With finite dissipation, transmittance is always an exponentially decaying function of thickness L; see also Fig. 2.

IV. DISCUSSION

We have shown that the reflection and refraction of the transverse electromagnetic waves at the boundary of the transparent isotropic chiral medium with frequencies ω around the longitudinal frequency ω_L have generic features familiar in crystal optics with circular dichroism. At a given frequency ω the overall picture is in general determined by the two circularly polarized waves in the medium with different relative refraction indices n_1 and n_2 ($n_2 \geqslant |n_1|$). The specific feature of this frequency range is that for $\omega > \omega_L$, both n_1 and n_2 are "ordinary" positive indices, while for $\omega < \omega_L$, one of the indices, n_1, is negative. The wave corresponding to this negative index has a negative group velocity, and its refraction behavior is largely typical of any negative-refraction material. The allowed region of $\omega < \omega_L$ is restricted from below, and at the bottom of this frequency range both transverse waves in the medium have a vanishing group velocity. A similar situation with two waves, one of positive and the other of negative group velocities, has been considered recently for nongyrotropic materials.[20] Based on their results, one could expect that in this case too negative group velocity waves would be contributing to focusing of light from a point source and the formation of an image upon transmission through a slab of the medium. In fact, recent calculations[15,16] demonstrated that a chiral medium slab can focus circularly polarized waves emitted by a point source.

It is interesting to note that, similarly to the case analyzed by Veselago,[1] the negative group velocity waves we consider appear in the region of frequencies that would be forbidden for electromagnetic waves—in the absence of magnetic resonance in Veselago's system and in the absence of chirality in ours. In Veselago's case, however, waves of both polarizations have negative group velocities while our system would exhibit negative group velocities for circularly polarized waves of one handedness only, the other one possessing ordinary positive group velocity dispersion.

We have demonstrated that the interesting region of frequencies around ω_L can be directly detectable in its frequency-dependent pattern of reflection of the polarized incident light. This however would not be the case for the normal incidence when the reflection is determined solely by the "average" refraction index $n=(n_1+n_2)/2$. [Likewise, the rotation of the plane of polarization of the normally incident wave in transmission is solely determined by the "detuning" of the indices, $\delta=(n_2-n_1)/2$.] It is the specular reflection that can display clear signatures owing to the fact that in the immediate vicinity of ω_L the wave with index n_1 does not propagate in the medium (similarly to the familiar total reflection phenomenon). At small incident angles, the n_1 wave starts to participate in refraction only for frequencies far enough from ω_L which would be featured in the reflection intensity.

The picture described above is quite general and should be applicable to various materials, whether in microwave or infrared and visible ranges of frequencies, provided that dissipation is weak enough. This restriction in fact leads to quite demanding requirements on the "allowed" magnitudes of gyrotropy (chirality) and dissipation. In addition to the dimensionless parameter γ', Eq. (13), the magnitude of the chirality can also be expressed through the observable rotatory power, Eq. (7):

$$\rho = \gamma' \omega_L/2c = \pi\gamma'/\lambda_0, \tag{50}$$

where $\lambda_0 = 2\pi c/\omega_L$ is the characteristic vacuum wavelength.

We will illustrate severity of dissipation-related requirements for materials describable by the oscillator resonance model, Eqs. (14) and (15). In that case, Eq. (19) particularly implies

$$\gamma' \gg 2\sqrt{\frac{\epsilon_b \Gamma}{\omega_L - \omega_T}} \tag{51}$$

for the dimensionless γ'. Let us take an example of a dielectric material in the IR region of optical vibrations assuming that $\epsilon_b = 3$, $\omega_L \simeq 1.6\times 10^{14}$ s^{-1} and $\omega_T \simeq 0.8\times 10^{14}$ s^{-1}. These values are similar to the IR data for MgO crystal in the region of frequency $\omega_T \simeq 400$ cm^{-1} where its dielectric constant has a resonance. Let us take the dissipative width of the resonance $\Gamma_T \simeq 1.6\times 10^{12}$ s^{-1} (that is, about 8 cm^{-1}). If one were to assume that the dissipative width Γ of transverse waves in the neighborhood of ω_L is the same, then requirement (51) amounts to at least $\gamma' > 0.5$ or $\gamma > 0.9$ μm. In terms of the rotatory power it would be necessary to have very large $\rho > 7.5$ deg/μm.

Similarly large values of needed γ' and even larger values of ρ can be estimated for sets of typical parameters characterizing excitonic transitions in organic crystals and plasmons in conducting media. These are indeed very tough demands if compared to the experimentally measured ρ in various solid-state chiral materials. Among possible candidates for appropriate chiral matrices may be organic materials such as polymers or molecules with helical structures like poly-L-lactic acid[29] and helicenes[30,31] or liquid crystals that exhibit very substantial rotatory powers. So for the films of the helical polymer poly-L-lactic acid the rotatory power at $\lambda = 632.8$ nm was reported[29] reaching 3.2 deg/μm (which is two orders of magnitude larger than that of quartz) corresponding to chirality parameter $\gamma \simeq 1.1$ nm. Clearly even such magnitudes of chirality would be insufficient to "overcome" the effects of dissipation unless the waves are actually less dissipative than the values used in our estimates. As is known, Γ is frequency dependent and becomes smaller away from resonances, which is in fact our case when $\omega_L - \omega_T$ is large. We should make a cautionary remark here that any reliable quantitative conclusions should be made based on the measured magnitude of chirality and dissipation for the appropriate range of frequencies. A great variation of the rotatory power as a function of frequency is well known and can, e.g., be seen in calculations for the particular case of helicenes.[31]

As has already been stressed, the spatial dispersion approach we are using is applicable phenomenologically to various ranges of frequencies. When using it, one does not need to separate the mean value of the microscopic current density $\mathbf{j}$ into two parts: dielectric $\partial\mathbf{P}/\partial t$ ($\mathbf{P}$ being the polarization) and magnetic $c\boldsymbol{\nabla}\times\mathbf{M}$ ($\mathbf{M}$ being the magnetization).[12] The latter explicit separation is a standard approach for describing artificial negative-refraction

metamaterials.[7] Particularly, this standard approach has been used in the recent references 3 and 13–16. In his proposal of a microstructured chiral metamaterial Pendry[3] provided several numerical examples for the resulting dispersion of microwaves in the region of the longitudinal frequency [we will be referring to the supporting online material (SOM) for that paper]. As our approach essentially uses very few parameters, it is therefore interesting to estimate the effective values of the model chirality parameter that would be corresponding to Pendry's examples. Our crude estimates are based on *visual* inspection of Figs. 8, 10, and 12 of SOM that correspond to different artificial structures. The longitudinal frequency $\omega_L/2\pi$ in all these examples is approximately within a 0.1–0.12-GHz interval and the depth $\Delta/2\pi$ of the minimum close to 0.013 GHz. A substantial difference in these examples is in the magnitude $k_{\min}$ (ranging within about 1.5–45 m^{-1}) of the wave vector corresponding to the minimum of the dispersion curve $\omega_-(k)$ (see our Fig. 1). As the dimensionless parameter γ' relates to $k_{\min}$ through $k_{\min} = \gamma' \omega_L/2c$, we extract this measure of the magnitude of chirality from Pendry's three examples as being very roughly (in the increasing order of this parameter) $\gamma' \simeq 2$, 6, and 40. With these γ' values, the chirality parameter is, respectively, $\gamma \simeq 0.8$, 2.5, and 17 m. The rotatory power at ω_L coincides with $k_{\min}$ and therefore would be measured in 10^2–10^3 deg/m.

Given the scarcity of available experimental data on the frequency-dependent rotatory power and dissipation in solid-state chiral materials, it is difficult at this stage to properly evaluate prospects and indicate candidates for natural materials where the phenomena described in this paper could be observable. From our tentative estimates, it is clear that material requirements are very challenging. It is not unlikely that better prospects might lie with artificial chiral metamaterials. In addition to the chiral structures discussed by Pendry[3] for microwaves, we will mention here that possibilities may be arising to build analogous structures on much smaller spatial scales utilizing such objects as conductive carbon tubule nanocoils[32] or twisted nanotube yarns[33] with tunable chirality. Such finer spatial size spiral structures could provide a more efficient chiral background for IR and visible domains. A recent progress should be noted on planar chiral metamaterials (see, e.g., Ref. 34 and references therein) that are capable of rotating polarization of the electromagnetic waves already in the visible domain.

ACKNOWLEDGMENTS

This work was supported by AFOSR Grant No. FA 9550-05-1-0409. V.M.A. thanks the Russian Foundation of Basic Research and Ministry of Science and Technology of Russian Federation for partial support. A.A.Z. is also thankful for a AFOSR/SPRING-Texas grant on negative refraction. The authors are grateful to R. H. Baughman and Y. R. Shen for discussions on chiral materials and negative refraction.

[1] V. G. Veselago, Sov. Phys. Usp. **10**, 509 (1968).
[2] A. Berrier, M. Mulot, M. Swillo, M. Qiu, L. Thylén, A. Talneau, and S. Anand, Phys. Rev. Lett. **93**, 073902 (2004).
[3] J. B. Pendry, Science **306**, 1353 (2004). For details referred to, see supporting online material at www.sciencemag.org/cgi/content/full/306/5700/1353/DC1
[4] J. B. Pendry, Contemp. Phys. **45**, 191 (2004).
[5] D. R. Smith, J. B. Pendry, and M. C. K. Wiltshire, Science **305**, 788 (2004).
[6] Y. Zhang and A. Mascarenhas, Mod. Phys. Lett. B **19**, 21 (2005).
[7] *Negative-Refraction Metamaterials*, edited by G. V. Eleftheriades and K. G. Balmain, (Wiley, Hoboken, NJ, 2005).
[8] L. I. Mandelstam, *Collection of Scientific Works* (Nauka, Moscow, 1950), Vol. 5, the 4th lecture given at Moscow State University in 1944.
[9] L. I. Mandelstam, Zh. Eksp. Teor. Fiz. **15**, 475 (1945).
[10] V. M. Agranovich and V. L. Ginzburg, *Crystal Optics with Spatial Dispersion, and Excitons* (Springer-Verlag, Berlin, 1984).
[11] V. M. Agranovich, Y. R. Shen, R. H. Baughman, and A. A. Zakhidov, Phys. Rev. B **69**, 165112 (2004).
[12] L. D. Landau and E. M. Lifshitz, *Electrodynamics of Continuous Media* (Butterworth-Heinemann, Oxford, 1984).
[13] S. Tretyakov, I. Nefedov, A. Sihvola, S. Maslovski, and C. Simovski, J. Electromagn. Waves Appl. **17**, 695 (2003).
[14] T. G. Mackay, Microwave Opt. Technol. Lett. **45**, 120 (2005).
[15] Y. Jin and S. He, Opt. Express **13**, 4974 (2005).
[16] C. Monzon and D. W. Forester, Phys. Rev. Lett. **95**, 123904 (2005).
[17] M. Born and K. Huang, *Dynamical Theory of Crystal Lattices* (Clarendon, Oxford, 1954).
[18] L. D. Barron, *Molecular Light Scattering and Optical Activity* (Cambridge University Press, Cambridge, England, 2004).
[19] V. M. Agranovich, Y. R. Shen, R. H. Baughman, and A. A. Zakhidov, J. Lumin. **110**, 167 (2004).
[20] L. Silvestri, O. A. Dubovski, G. C. L. Rocca, F. Bassani, and V. M. Agranovich, Nuovo Cimento Soc. Ital. Fis., C **27**, 437 (2004).
[21] A. A. Golubkov and V. A. Makarov, Phys. Usp. **38**, 325 (1995).
[22] A. P. Vinogradov, Phys. Usp. **45**, 331 (2002).
[23] D. Bedeaux, M. Osipov, and J. Vlieger, J. Opt. Soc. Am. A **12**, 2431 (2004).
[24] S. I. Pekar, Sov. Phys. JETP **6**, 785 (1958).
[25] V. L. Ginzburg, Sov. Phys. JETP **7**, 1096 (1958).
[26] V. M. Agranovich and V. I. Yudson, Opt. Commun. **9**, 58 (1973).
[27] M. P. Silverman, J. Opt. Soc. Am. A **3**, 830 (1986).
[28] S. Bassiri, C. H. Papas, and N. Engheta, J. Opt. Soc. Am. A **5**, 1450 (1988).
[29] Y. Tajitsu, K. Makino, A. Saito, M. Ebina, M. Okuno, Y. Shikinami, M. Date, and E. Fukada, J. Mater. Sci. Lett. **19**, 1537 (2000).
[30] R. H. Martin and V. Libert, J. Chem. Res., Synop., 130 (1980).

[31] V. Buss and K. Kolster, Chem. Phys. **203**, 309 (1996).
[32] M. Zhang, Y. Nakayama, and L. Pan, Jpn. J. Appl. Phys., Part 2 **39**, L1242 (2000).
[33] M. Zhang, K. R. Atkinson, and R. H. Baughman, Science **306**, 1358 (2004).
[34] W. Zhang, A. Potts, A. Papakostas, and D. M. Bagnall, Appl. Phys. Lett. **86**, 231905 (2005).
[35] See pictures on p. 252 of Ref. 10.